Optical Microscopy Studies of Dynamics within Individual Polymer-Dispersed Liquid Crystal Droplets

DANIEL A. HIGGINS,* JEFFREY E. HALL, AND
AIFANG XIE

*Department of Chemistry, Kansas State University,
Manhattan, Kansas 66506*

Received July 27, 2004

ABSTRACT

Optical devices based on polymer-dispersed liquid crystal (PDLC) thin films derive their functional properties from the electric-field-induced reorientation of (sub)micrometer-sized polymer-dispersed liquid crystal (LC) droplets. In these materials, the LC reorientation dynamics are strongly dependent on droplet size and shape, as well as polymer/LC interfacial interactions. The dynamics also vary spatially within individual droplets. This Account describes studies of individual PDLC droplets and their field-induced dynamics by high-resolution near-field scanning optical microscopy (NSOM) and multiphoton-excited fluorescence microscopy (MPEFM). Included are studies of native ("pure") PDLCs and those doped with ionic compounds and dyes; the latter are used in sophisticated photorefractive materials.
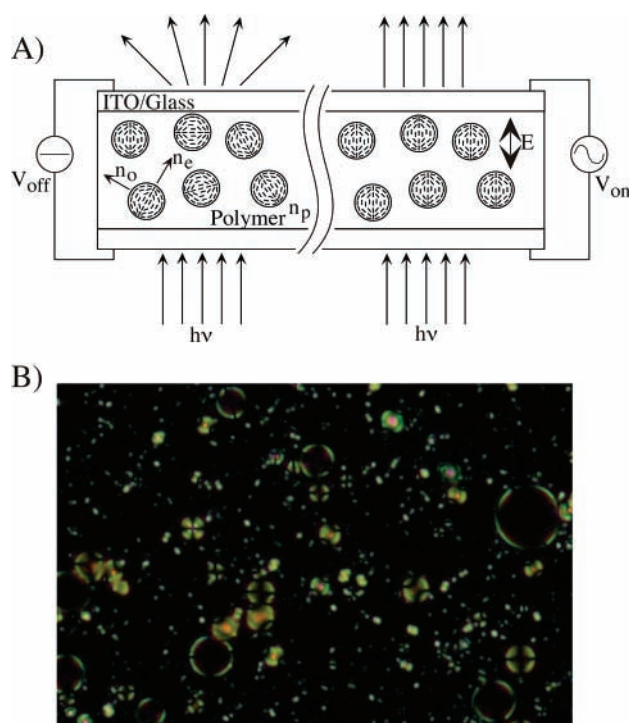
Introduction

Polymer-dispersed liquid crystal (PDLC) thin films find a variety of applications in a range of optical devices. These include their use in electrically switchable windows, optical shutters, flexible displays, diffractive optics, and photorefractive systems.[1–5] PDLCs consist of (sub)micrometer-sized birefringent LC droplets encapsulated within what is usually an optically transparent polymer. Figure 1 shows a schematic cross-section of a PDLC device and a polarized light micrograph of a PDLC film. The molecular organization within the encapsulated LC droplets depends on the elastic constants of the LC and the interfacial anchoring conditions.[3–6] In their native state, the fast (or slow) optical axes of these droplets are usually randomly aligned, causing the materials to strongly scatter light. Pure polymer/liquid-crystal composites are translucent in this state, while dye-doped versions[7] can be completely opaque. When polymers and LCs with proper

FIGURE 1. Panel A presents a model cross-section of a PDLC device. The refractive index of the polymer is n_p, while those of the LC are n_e and n_o. Panel B presents a far-field optical birefringence micrograph of a PDLC film.

refractive indices are employed, application of an electric field causes the films to become optically transparent to normally incident light. This field-induced change results from reorientation of the LC directors within the droplets.

An important attribute of PDLC-based optical devices includes the ease by which they are fabricated. PDLC materials are often prepared by emulsion techniques and by temperature-, polymerization-, or solvent-induced phase separation.[1–5] Thin PDLC films can be cast onto suitable conductive, transparent substrates. In functional devices, only a few volts per micrometer of film thickness are needed to induce optical switching. PDLC systems draw very little current in the powered state. Optical contrast in PDLCs comes predominantly from their inherent light-scattering properties. No complicated surface treatments or external optics (i.e., polarizers) are required to make a functioning device.

While commercial devices are already being produced from PDLCs, their chemical and physical properties are not yet completely understood. An area of particular concern is in the understanding of electric-field-induced LC dynamics. Prior research has proven the existence of spatial and temporal complexities in LC droplet reorientation.[8] In early studies, UV–vis absorption and light-scattering methods were used to monitor the LC dynamics.[8–10] More recently, nuclear magnetic resonance,[11–14] Fourier transform infrared spectroscopy,[15,16] and several time-resolved microscopies and spectroscopies have been

Daniel A. Higgins received a B.A. in chemistry from St. Olaf College (Northfield, MN) in 1988 and a Ph.D. in chemistry from the University of Wisconsin-Madison in 1993. He subsequently worked as a NSF postdoctoral fellow under Prof. Paul F. Barbara. In 1996, he joined the faculty at Kansas State University, where he is an associate professor.

Jeffrey E. Hall received a B. A. in chemistry from Northwestern College (Orange City, IA) in 1999 and a Ph.D. in Chemistry from Kansas State University in 2004, working under the direction of Daniel Higgins.

Aifang Xie received B.S. and M.S. degrees in physics from Henan Normal University (China) in 1996 and 1999, respectively, and a Ph.D. in physics from the Chinese Academy of Sciences (Beijing) in 2002. She is presently working as a postdoctoral associate with Daniel Higgins.

* Corresponding author. E-mail: higgins@ksu.edu.

employed.[17−20] All such methods yield valuable information on the LC dynamics but do not provide sufficient spatial resolution to resolve the reorientation dynamics within individual LC droplets.

This Account describes work from our labs in which we have been using novel optical microscopic techniques such as near-field scanning optical microscopy (NSOM)[21−30] and multiphoton-excited fluorescence microscopy (MPEFM)[31−34] to study individual polymer-dispersed LC droplets and their electric-field-induced dynamics. NSOM provides high-resolution optical images of the droplets and their dynamics, as well as topographic information, allowing for development of detailed correlations between droplet size/shape attributes and the dynamics. MPEFM methods provide complementary capabilities, yielding somewhat lower spatial resolution but providing the ability to probe droplet organization and dynamics deep within functional PDLC devices. These methods have provided images with sub-diffraction-limited resolution of spatial variations in the LC droplet dynamics. Models describing the origins of these variations are used to explain the results.
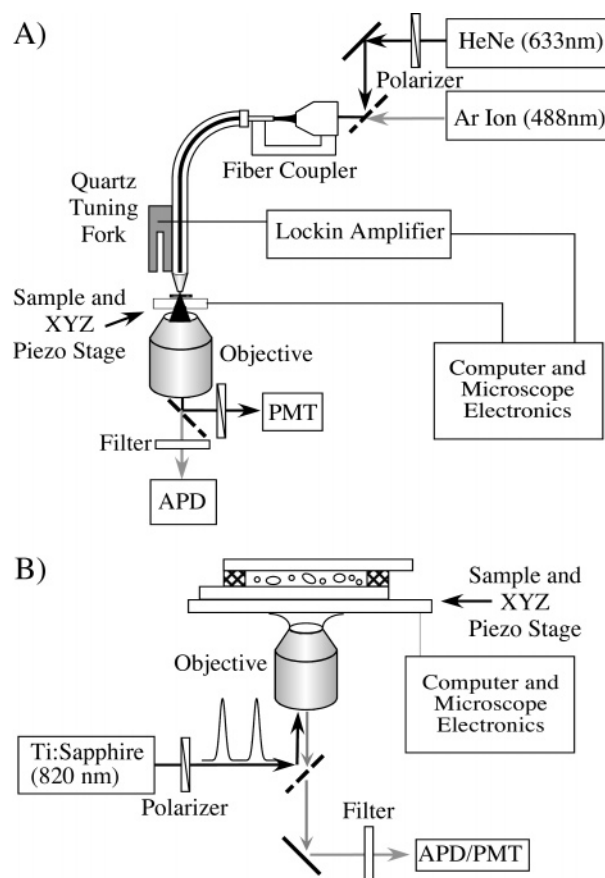
Optical Microscopy

Near-Field Scanning Optical Microscopy. NSOM methods are described in detail elsewhere.[35] Here, only the basic principles are discussed, along with the unique methods employed in our labs.

NSOM has been used to characterize both pure[21−23,25] and dye-doped[26−30] PDLC films. These studies allowed for the location and organization of LC and dye dopants to be determined and for correlation of these attributes with droplet shape and sample morphology. Novel methods developed in our laboratory[22] were then employed to study electric-field-induced LC, dye, and ion dynamics within individual PDLC droplets.

Figure 2A shows a schematic of the aperture-based NSOM instrument employed. During imaging, the sample is illuminated with linearly polarized light from a sub-wavelength-sized aluminum-coated fiber optic probe. Images are acquired by raster scanning the sample beneath the probe. To obtain high-resolution optical images, the tip and sample must be maintained in close proximity, and hence, the sample topography must be followed. In optical imaging of PDLCs, the light exiting the probe passes through the birefringent LC droplets, which modify the polarization state. Optical contrast is obtained by detecting the transmitted light under crossed-polarization conditions. The simultaneous recording of optical and topographic information makes NSOM a particularly powerful tool for characterizing PDLC sample structures.

In dynamic NSOM imaging studies, the aluminum-coated probe is electrified, as is the conductive, transparent substrate upon which the sample is cast. A modulated electric field is applied between the probe and sample, inducing LC reorientation. Changes in the optical birefringence signal due to LC reorientation are monitored

FIGURE 2. Panel A shows the components of the near-field scanning optical microscope. Panel B shows the components employed in the sample scanning multiphoton-excited fluorescence microscope.

using a lock-in amplifier or an oscilloscope. Spatial or temporal resolution of the LC dynamics or both are readily obtained. Importantly, the use of the sharp NSOM probe for field application helps confine the induced dynamics to the near-field regime,[25] even in optically thick samples.

In dye-doped PDLCs,[26−28,30] the materials are characterized as described above with the option of simultaneously obtaining fluorescence images of the sample as well. Fluorescence is induced by simultaneously coupling light of a second wavelength into the NSOM probe and using it to excite the dyes. Separate optical detectors independently monitor the fluorescence and birefringence signals.

Multiphoton-Excited Fluorescence Microscopy. The necessity to maintain the tip and sample in close proximity makes NSOM studies of PDLC devices difficult. Conventional far-field light microscopy can also be difficult because of strong light scattering. MPEFM is a nonlinear optical imaging method that overcomes many such limitations and has been extensively described in the literature.[36,37] Figure 2B depicts the most important components of our microscope.

Our MPEFM system is built upon a conventional epi-illumination microscope. Pulses of light from a Ti:sapphire laser ($\lambda > 800$ nm) are directed into the microscope and focused to a diffraction-limited spot within the sample using a high-numerical-aperture objective. In PDLCs
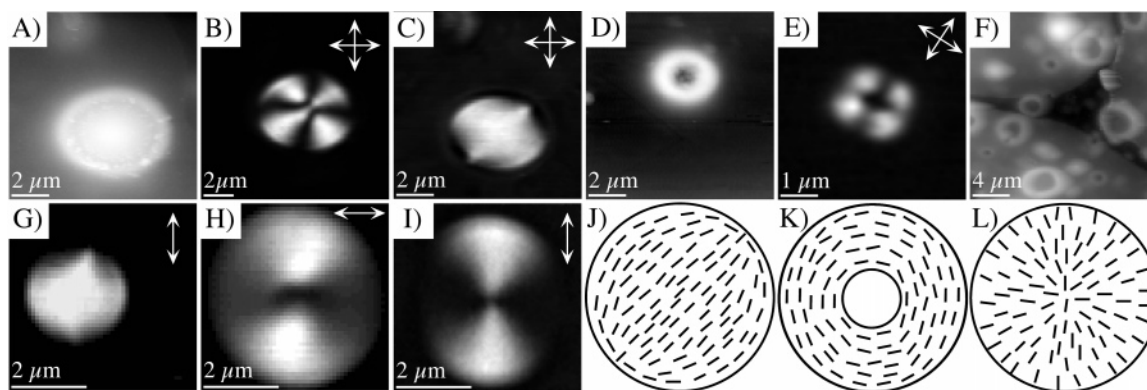
FIGURE 3. Images and models of several LC droplets. Panel A shows a topographic image of an ellipsoidal droplet. Panels B and C show NSOM birefringence images of two bipolar ellipsoidal droplets having optical axes oriented perpendicular and parallel to the film plane, respectively. Panel D shows a topographic image of a collapsed ("toroidal") droplet. Panel E shows the NSOM birefringence image of the droplet shown in panel D. Panel F shows a topographic image of a dye-doped PDLC sample showing several collapsed droplets. Panels G and H show MPEFM images of bipolar and toroidal droplets, respectively. Panel I shows a MPEFM image of a PDLC droplet of radial configuration. Panels J–L show models for the LC organization in bipolar, toroidal, and radial droplets, respectively. Appended arrows show the incident and detected polarizations.

employing cyanobiphenyl and terphenyl LCs, fluorescence arises from three-photon excitation of the molecules.[31] Images are collected by raster scanning the sample, which is mounted above the objective on a piezo-electrically driven stage, while the emitted fluorescence is detected.

The use of near-IR light for fluorescence excitation has several advantages in studies of light-scattering, birefringent materials. First, because light scattering depends on the optical frequency to the fourth power, scattering of the incident laser light is minimized. Changes in the polarization state of the incident light by passage through the birefringent droplets are also minimized because the LC is less birefringent at longer wavelengths and the optical path through the droplets is shorter relative to the wavelength of light.

Perhaps most important from the perspective of optically thick PDLC devices, fluorescence is excited only in the focal volume of the microscope. MPEFM images are virtually background-free, and depth-profiling experiments are readily performed by simply changing the focus depth. Multiphoton excitation is also highly sensitive to molecular orientation, so MPEFM can also be used to obtain the LC organization and to measure local order parameters.[33]

Dynamical information was obtained in MPEFM studies by preparing functional PDLC films between conductive glass substrates or with embedded copper wires. An electric field was applied to the sample (either perpendicular or parallel to the film plane), and changes in the LC fluorescence were recorded in time as a function of position within the droplets. Time-resolved fluorescence movies of the reorientation process were then prepared, depicting dramatic spatial variations in the LC dynamics.

Droplet Shape Characteristics and Liquid Crystal Organization

In the majority of PDLC devices, the encapsulated LC droplets are meant to serve as efficient light-scattering centers.[38] In practical devices, droplets having diameters of about 1 μm and a narrow size distribution work best.[39,40] Droplet shape is also important because it can cause LC organizational changes and plays a significant role in governing LC reorientation dynamics.[8,10] Unfortunately, droplet size and shape attributes often vary substantially from droplet to droplet, leading to significant sample heterogeneity.

PDLC film optical properties are often modeled based on the assumption of spheroidal or ellipsoidal droplets of a specific size. Figure 1B shows an optical micrograph of a PDLC thin film comprised of a common LC mixture (E7) dispersed in a poly(vinyl alcohol) (PVA) matrix. As is readily apparent, the droplets take on a wide range of sizes and exhibit significant variability in the LC organization.

NSOM and MPEFM methods have been applied in our labs to better understand the droplet shape classes and LC organizations present in such materials. Figure 3 shows a series of images that depict some of the different types of droplets that have been observed. Figure 3A–C depict NSOM images of the expected spheroidal or ellipsoidal droplets for the E7–PVA system. The LC in these droplets is organized in the bipolar configuration, as depicted in Figure 3J. Figure 3D–F, however, show topographic and optical NSOM images of unexpected "collapsed" or "toroidal" droplets,[23,31] the latter exhibiting images consistent with the LC organization shown in Figure 3K. Figure 3G,H depicts MPEFM images of a bipolar ellipsoidal droplet and a "toroidal" droplet, respectively. Our results have shown that a significant fraction (~8% of droplets) in pure E7–PVA films take on a "toroidal" shape.[31] Studies performed for dye-doped[28] and surfactant-treated[31] materials prove that a reduction in interfacial energy can cause an increase in the fraction of collapsed or "toroidal" droplets. Although not yet proven, the appearance of the "toroidal" droplets likely results from competition between surface energy effects, which tend to yield spheroidal droplets, and LC organizational energy, which favors droplets having no organizational defects (i.e., as occur at the poles of bipolar droplets).

Finally, Figure 3I,L presents a view of how polymer/ LC interfacial interactions alter the LC organization and hence the images obtained. These data are for a droplet of radial configuration,[34] resulting from perpendicular LC anchoring at a poly(isobutyl methacrylate) surface.

Controlling Liquid Crystal Droplet Shape

In most PDLC film preparations, droplet size and shape are uncontrolled, leading to broadly distributed sample properties.[1−5] Dramatic improvements in the properties of PDLC-based devices may be achieved by preparing materials with well-controlled droplet sizes and shapes. We recently demonstrated a method for obtaining highly regular LC droplets that can also be used to prepare well-ordered hexagonal droplet arrays.[32] In this method, templated voids are prepared in a polymer film, and the voids are subsequently filled with LC.

This method is outlined in Figure 4A and is based on well-known methods for producing inverse opals.[41] First, monodisperse polystyrene microspheres were deposited onto a glass substrate. The spheres were then coated with a water-soluble polymer such as PVA or poly(ethylene oxide). After drying, the microspheres were removed by immersion in chloroform or toluene. This procedure left behind a polymer film containing templated voids of the same size, shape, and organization as the microspheres. The templated polymer film was then covered with a second substrate and capillary action was used to load the voids with LC. Related materials in which the voids between the microspheres have been filled with LC have also been described,[42] but to our knowledge, this was the first time PDLC films had been fabricated in this manner.

Figure 4 shows MPEFM images of hexagonally ordered templated PDLC droplet arrays. Figure 4B was recorded using circularly polarized incident light to minimize contrast caused by polarization-dependent excitation of LC fluorescence. Such images most clearly depict the hexagonal order. In subsequent studies, linearly polarized light was used to excite LC fluorescence in hopes of understanding LC organization within the templated droplets.[32] Of primary interest in these studies were orientational correlations observed between neighboring droplets. Figure 4D shows a MPEFM image recorded using linearly polarized incident light. Simulations of the three-photon excited images obtained from bipolar PDLC droplets under different polarization conditions are shown in Figure 4C. Surprisingly, the optical (or polar) axes of many droplets in Figure 4D are oriented in the same direction. The white box appended to the image highlights a region in which ~16 droplets possess nearly identical LC alignment: all are nearly perpendicular to the incident polarization. Figure 4E depicts the approximate optical axis alignments for many droplets in this region. These results prove that LC organization is well correlated over long distances in these materials. Such correlations could arise from (I) subtle compression of the void array along a particular direction due to compression of the precursor sphere arrays, (II) organizational "communication" be-
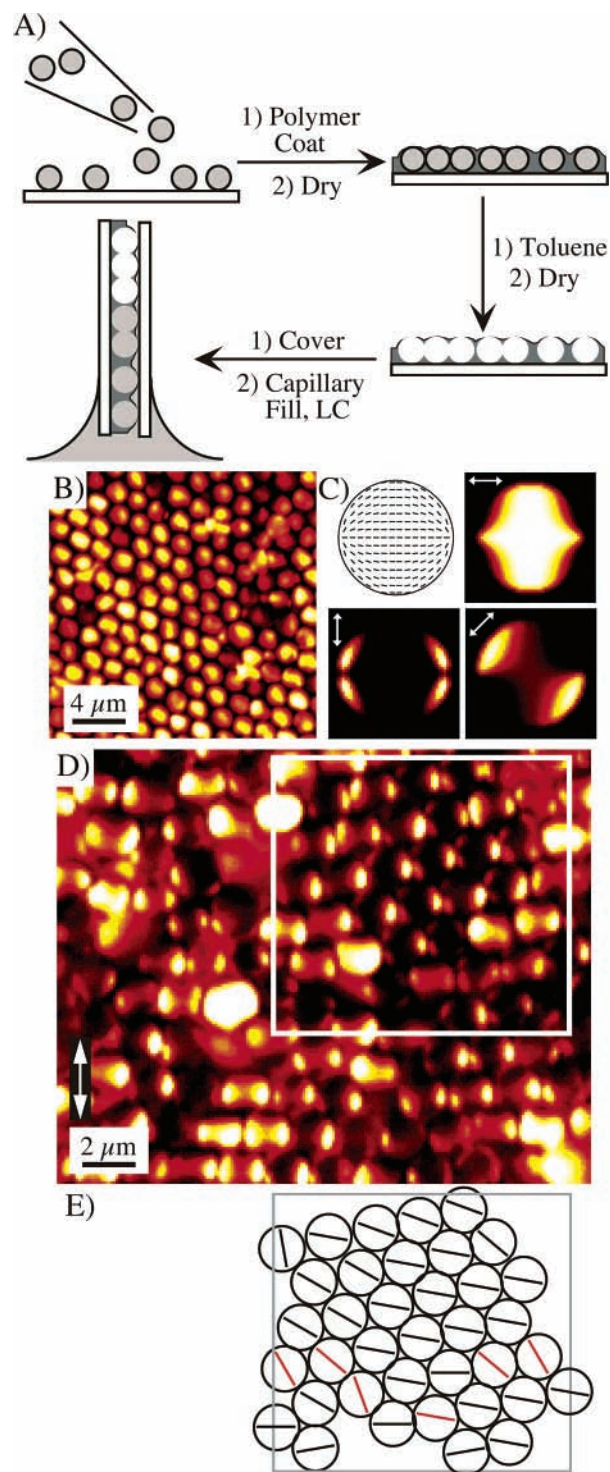
FIGURE 4. Panel A shows a schematic of the PDLC templating method. Panel B shows a MPEFM image of a templated, hexagonally ordered LC droplet array. Panel C shows the model configuration and simulated three-photon excited fluorescence images for bipolar droplets under different incident polarization conditions (see appended arrows). Panel D shows a MPEFM fluorescence image of templated PDLC droplets recorded using linearly polarized light, and panel E shows a model for droplet alignment in the highlighted region.

tween droplets through interconnecting channels between the voids, (III) alignment induced by physical features on the covering glass slide, or (IV) a combination of these

factors. Mechanism III was verified by inducing LC alignment by rubbing polymer-coated cover slides prior to assembly of the devices.[32] However, evidence for the participation of the other mechanisms also exists. Included are the dramatic droplet-to-droplet variations in LC alignment for droplets positioned near grain boundaries or single void defects.

Since our initial report on these materials, researchers at Bell Labs have prepared 3D droplet arrays using similar methods and have demonstrated Bragg diffraction from them.[43] Should it become possible to prepare well-ordered hexagonal arrays over large areas,[41] such materials may someday lead to revolutionary, switchable Bragg devices based on PDLCs.

Dynamics in Pure Polymer/Liquid-Crystal Composites

Obtaining detailed, high-resolution images of the electric-field-induced dynamics[8,10] within single LC droplets has been a long-term goal of our research.[21,22,24,25,33,34] These results, coupled with detailed theoretical modeling, will allow for the complete understanding of how polymer-encapsulated LC droplets respond to applied electric fields.

Figure 5 presents typical topography and dynamic NSOM images obtained from pure, bipolar PDLC droplets. The amplitude images shown in Figure 5B,C reflect the changes in LC alignment induced locally by the modulated electric field. Figure 5E depicts a line profile taken from the image in Figure 5B. Sub-diffraction-limited resolution is clearly obtained, indicating that the dynamics probed occur within the near field of the NSOM tip, even though the droplets are approximately 1 μm thick.[25] The sensitivity of these measurements to near-field effects arises in part from concentration of the applied electric field near the end of the sharp aluminum-coated NSOM probe.[22,25]

Contrast in the amplitude images depends on the relaxed LC orientation and the optical thickness of the droplet region being probed. Phase images (see Figure 5D) provide a better depiction of the droplet dynamics, because of their reduced sensitivity to these parameters. Clearly visible in Figure 5D are dramatic spatial variations in the phase signal. These phase images and complementary time-resolved data[21] obtained from numerous bipolar droplets indicate that the LC dynamics are faster near the polymer−LC interface and relatively slower in central droplet regions. They also suggest that the LC reorientation process can be quite complex in central regions, especially near the equatorial plane and polar axes of bipolar droplets. LC reorientation is more rapid in outer droplet regions due to the greater elastic torques active in these regions.[25,33] Over the equatorial plane, the droplet polar axis, or both, dynamical differences arise primarily from reduced coupling of the LC to the applied field (because the relaxed LC lies perpendicular to the field).[25,33] Reorientation in these regions is driven by reorientation of neighboring LCs, and frequency-dependent studies
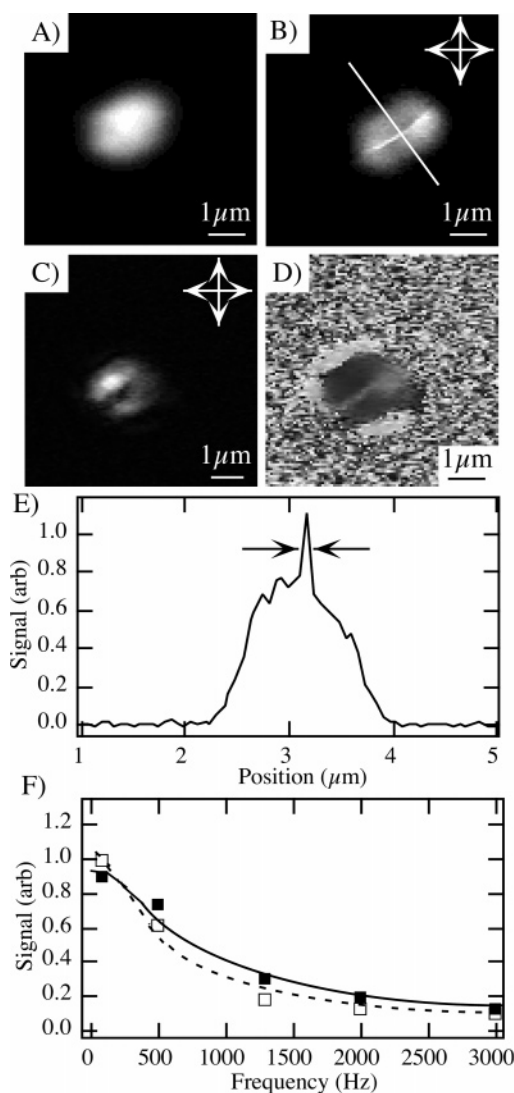
FIGURE 5. Panel A shows a NSOM topography image of a PDLC droplet. Panels B and C show NSOM dynamic amplitude images recorded at high and low field modulation frequencies (3000 and 100 Hz), respectively. Panel D shows the NSOM dynamic phase image collected simultaneously with the image shown in panel C. Panel E shows a line profile from panel B. Panel F shows NSOM dynamic amplitude signals for points on (■) and off (□) the central axis.

(Figure 5F) can be used to obtain information on the relative importance of the local viscous and elastic torque densities in governing reorientation in these regions.[25]

Representative MPEFM movies of the dynamics in bipolar[33] and radial[34] droplets are shown in Figures 6 and 7, respectively, along with time transients recorded for specific droplet regions. In the case of the bipolar droplet (Figure 6), features associated with the equatorial plane and polar axis dynamics are clearly depicted. The polar axis in this droplet runs from the lower left corner of the images to the upper right. Unlike the NSOM data, these data were recorded under the influence of a relatively uniform applied electric field, indicating that these dynamical features reflect inherent droplet properties variations. As observed by NSOM, the LC relaxation dynamics are fastest in the outer circumference (especially away
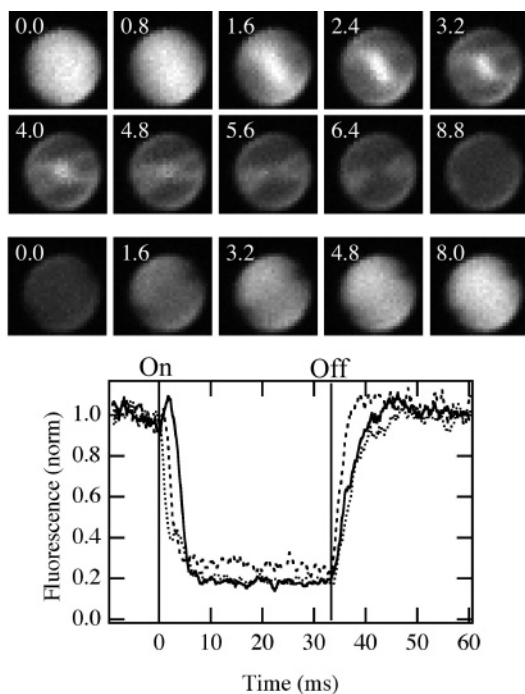
FIGURE 6. The top panel shows representative frames from a MPEFM movie of PDLC droplet dynamics in a bipolar LC droplet. The dynamics after application of the electric field are depicted in the first two rows. The dynamics after removal of the field are shown in the last row. The time in milliseconds after field switching is given. The bottom panel shows time transients recorded for single positions over the droplet. Data are shown from center (—), equatorial/edge (— — —), and polar (···) regions. The times at which the field was switched on and off are shown.

FIGURE 7. The top panel shows representative frames from a MPEFM movie of PDLC droplet dynamics in a radial LC droplet. The dynamics after application of the electric field are depicted in the first row. The dynamics after removal of the field are shown in the last two rows. The time in milliseconds after field switching is given. The bottom panel shows time transients recorded for single positions over the droplet. Data are shown from center (···), interfacial (— — —), and intermediate (—) regions. The times at which the field was switched on and off are shown.
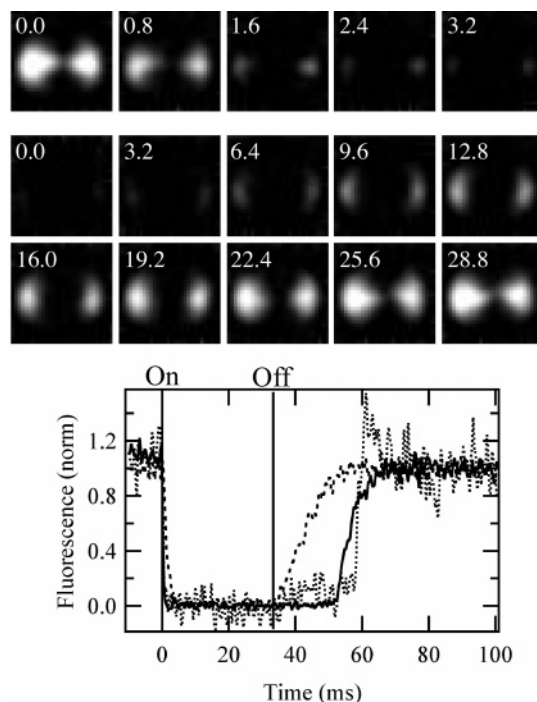
from the poles) of the droplet, where relaxation is driven by orientationally "anchored" interfacial LC.[33]

Figure 7 depicts radial droplet dynamics recorded using an alternative geometry in which the electric field was applied parallel to the film plane. Aside from demonstrating that different experimental geometries are possible using MPEFM methods, these data also depict how the relaxation process depends on the droplet shape attributes and LC organization. In this radial droplet, a long onset prior to LC relaxation in central droplet regions is observed, due to relaxation through a metastable "axial" configuration upon removal of the applied field.[34]

Dynamics in Dye-Doped and Photorefractive PDLCs

Dyes and other dopants are often employed in PDLC-based optical shutters and photorefractive materials.[7,44] By design, these additives alter the film properties, giving the devices their functional attributes (e.g., a photoinduced change in refractive index in the case of photorefractives). In a number of recent publications, we have explored the influence of both permanent[24,30] and photogenerated[27,29,30] ions on PDLC droplet dynamics.

Figure 8 shows dynamic NSOM images acquired from a PDLC sample doped with photoexcitable electron-donating and -accepting dyes. The droplet shown contains millimolar levels of perylene (photoexcitable electron

donor) and a naphthalene diimide (electron acceptor).[45] These dyes were chosen based on their prior use in photorefractive materials.[44,46] Our NSOM studies yielded information on the origins of the photorefractive effect in individual PDLC droplets and also pointed to a possible new method for enhancing the photorefractive effect in PDLCs.

PDLCs doped with the dyes alone show only subtle effects of ion generation in NSOM experiments. The sample shown in Figure 8, however, was also doped to 11 μM with tetrabutylammonium tetrafluoroborate.[30] Addition of these permanent ions causes enhanced sensitivity of the NSOM dynamics signals to photogenerated ions. We have also shown that the added ions yield a corresponding increase in the photorefractivity of bulk PDLCs.[30] Figure 8A,D,G shows phase images recorded before, during, and after ion generation, respectively. Photogeneration of ions was induced using 488 nm light, while the LC dynamics were monitored using 633 nm light. During ion generation, the average phase angle measured increased by 19° ± 3° (Figure 8D relative to Figure 8A), a much larger increase than was observed in the absence of permanent ions, where the increase typically averaged ~2°. Experiments performed on several samples proved this to be a general trend. After ion generation, the phase angle returned to within 2° ± 2° of its value prior to ion
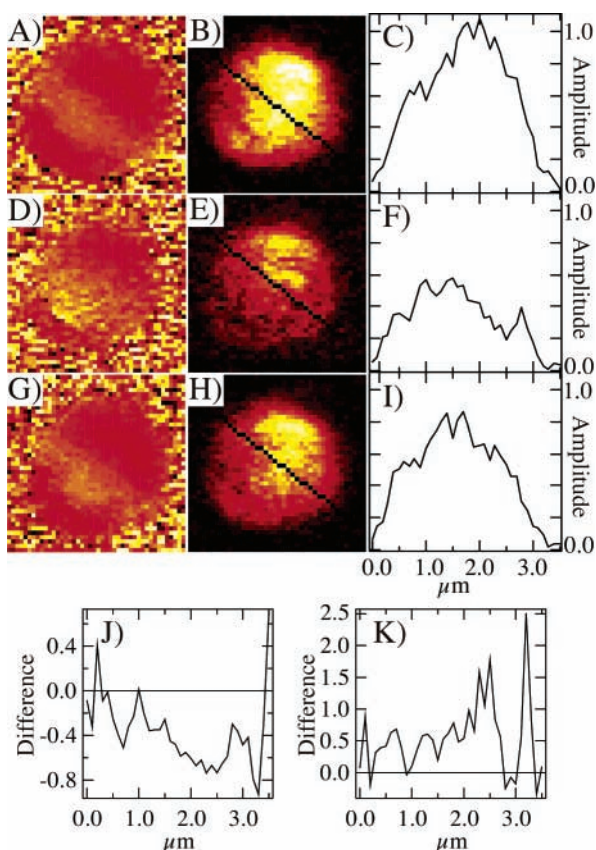
FIGURE 8. Panels A and B show NSOM dynamic phase and amplitude images of a photorefractive-PDLC droplet prior to photogeneration of ions. Panel C shows the line profile from the image in panel B. Panels D and E show NSOM phase and amplitude images recorded for the same droplet during photogeneration of ions. Panel F shows the line profile from the image in panel E. Panels G and H show phase and amplitude images acquired after ion generation. Panel I shows the line profile from the image in panel H. Panels J and K show changes in the amplitude signal between images recorded during and before ion generation and after and during ion generation, respectively.

generation, indicating that most of the photogenerated ions recombined or were otherwise removed.

Amplitude images (see Figure 8) exhibit similar sensitivity enhancements in the presence of permanent ions.[30] These images are shown in Figure 8B,E,H. Line profiles taken from these images are reported in Figure 8C,F,I and their relative differences are shown in Figure 8J,K. The line profiles most clearly demonstrate the magnitude of the changes in signal amplitude and a view of the spatial variations therein resulting from ion photogeneration. The decrease in signal amplitude during ion generation was most pronounced in the droplet center, where the amplitude decreased by ~60%. This spatial dependence likely arises from the movement of ions to droplet regions closest to the electrode surfaces. Hence, ion-induced LC relaxation occurs most strongly in central droplet regions.

Several possible mechanisms exist by which permanent ions might improve the sensitivity of the NSOM experiments to photogenerated ions and enhance bulk photorefractivity. First, the ions may stabilize the photogenerated, charge-separated radical ions,[47,48] resulting in a more

rapid and complete cancellation of the applied electric field and, hence, enhanced LC relaxation. Second, they may cause a change in the diffusion coefficients of either ionic product, resulting in larger space−charge fields.[44] While these two mechanisms are well-known and have been previously described, a third possible explanation also exists that, to our knowledge, has not previously been addressed. This mechanism involves the nonlinear dependence of LC alignment on the local electric-field strength, which is determined in part by the ions present (whether permanent or photogenerated).

Computer simulations were performed to better understand the contributions of this latter mechanism[30] and the overall dynamics of ion-dependent LC relaxation. One-dimensional simulations of the dynamics associated with ion migration, space−charge field formation, and LC reorientation were performed using finite difference time domain methods.[27] As in the experimental studies, the sample was exposed to a sinusoidally modulated, externally applied electric field. Ion concentrations similar to those used experimentally were employed. Simulated optical signals were obtained and their amplitude and phase characteristics determined, exactly as with the experimental data.

Figure 9 gives representative results from these simulations, depicting the influence of increased ion concentrations. These particular simulations employed a 200 Hz field modulation frequency. Figure 9A depicts the squared electric field within a droplet containing 1 μM ions. The field data are plotted with respect to time and position within the droplet, relative to the polymer/LC interface (at 0.0 nm). The electric field in the droplet remains relatively uniform throughout and has a relatively small amplitude (peak at ~2 V/μm). Figure 9B illustrates the squared electric field in a droplet containing 30 μM ions. In this case, the electric field within the droplet shows dramatic spatial and temporal variations. The field in the central regions of the droplet peaks below 2 V/μm, while the field at the interface peaks at ~5.3 V/μm, later in time. These variations reflect the buildup and decay of an ion-dependent space−charge field at the polymer/LC interface.

The time-dependent LC orientation and simulated NSOM signals were determined from the field data. Figure 9C plots the resulting simulated optical signals for 1 μM ions (solid line) and 30 μM ions (dashed line). Also shown on this plot is the approximate LC orientation state at each point during the simulation. The modulated optical signal (resulting from LC reorientation) clearly shifts earlier in time (i.e., there is a smaller phase lag) as the ion concentration increases. Simultaneously, a decrease in the signal amplitude also occurs. These observations are identical to those obtained in NSOM experiments (Figure 8). Most importantly, simulations performed for a series of ion concentrations also predict an increase in the sensitivity of the dynamic NSOM experiments to photogenerated ions for samples of higher average ion concentrations (see Figure 9D).
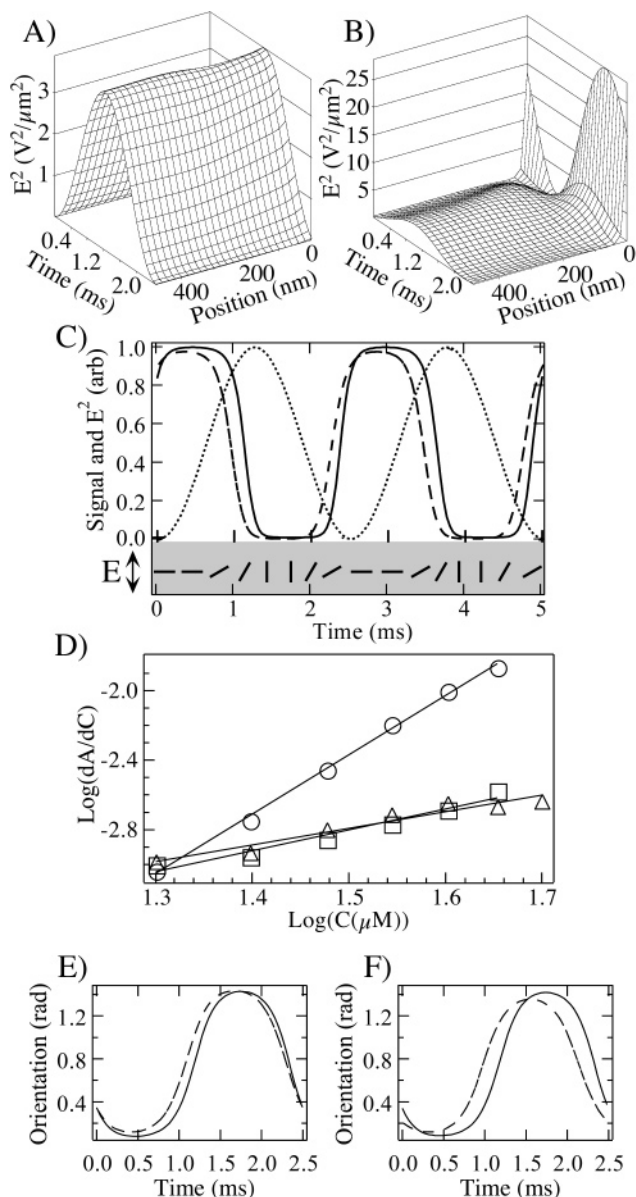
FIGURE 9. Simulated squared electric field in a droplet with (A) 1 μM ions and (B) 30 μM ions as a function of time and position within the droplet (polymer/LC interface at 0.0 nm). Panel C shows the simulated optical signal from an ion-doped LC droplet. Data are shown for ion concentrations of 30 ($- - -$) and 1 μM (—), as is the applied squared electric field ($\cdots$). The lower portion of the figure depicts how the LC reorients during the field cycle. Panel D shows the simulated change in the NSOM signal amplitude for a small change in ion concentration (dA/dC) as a function of the average ion concentration. Shown are results for field modulation frequencies of 100 (◯), 200 (☐), and 400 Hz (△). Panels E and F show simulated LC orientation angles at the polymer/LC interface and in the center of the droplet, respectively, for ($- - -$) 30 μM ions and (—) 1 μM ions.

The spatial variations in LC dynamics contributing to the NSOM signals can be better understood by looking at the LC orientation angle at different positions within the droplet.[30] Figure 9E,F shows the LC orientation as a function of time at the droplet surface and in the droplet center, respectively, for 1 and 30 μM ion concentrations. An orientation angle of 0.0 rad corresponds to the fully relaxed (zero-field) orientation of the LC, and $\pi/2$ corresponds to field-aligned LC. The LC reorientation process in the droplet center clearly changes more dramatically with a change in ion concentration than it does near the droplet surface. The modulated LC orientation in the droplet center is more strongly damped at higher ion concentrations because of the more rapid decay of the electric field within the droplet under these conditions. Hence, most of the changes in the NSOM signals observed in Figure 8 can be attributed to changes in the LC reorientation process deep within the droplet, as can the LC relaxation that drives the photorefractive effect in PDLCs.

Conclusions

The dynamics of electric-field-induced LC droplet reorientation play an important role in governing the functional properties of PDLC-based devices. Such dynamics are highly dependent on droplet size and shape, as well as interfacial anchoring conditions. Even in systems of highly regular droplets, the dynamics vary internally within individual droplets due to the complex cooperative mechanisms of field-induced LC reorientation. Proper microscopic methods with sufficient spatial resolution are required to probe these dynamics and fully understand the mechanisms by which LC reorientation occurs. NSOM and MPEFM are two techniques that meet these requirements and provide complementary information on PDLC thin film morphology and dynamical properties.

References

(1) Doane, J. W.; Vaz, N. A.; Wu. B.-G.; Zumer, S. Field Controlled Light Scattering from Nematic Microdroplets. *Appl. Phys. Lett.* **1986**, *48*, 269−271.
(2) Drzaic, P. S. Polymer Dispersed Nematic Liquid Crystal for Large Area Displays and Light Valves. *J. Appl. Phys.* **1986**, *60*, 2142−2148.
(3) Doane, J. W. *Liquid Crystals: Applications and Uses*; World Scientific: Singapore, 1990; Vol. 1.
(4) Kitzerow, H. S. Polymer-Dispersed Liquid Crystals. From the Nematic Curvilinear Aligned Phase to Ferroelectric Films. *Liq. Cryst.* **1994**, *16*, 1−31.
(5) Crawford, G. P.; Doane, J. W.; Zumer, S. Polymer Dispersed Liquid Crystals: Nematic Droplets and Related Systems. In *Handbook of Liquid Crystal Research*; Collings, P. J., Patel, J. S., Eds.; Oxford University Press: New York, 1997; pp 347−414.
(6) Coates, D. J. Polymer-Dispersed Liquid Crystals. *J. Mater. Chem.* **1995**, *5*, 2063−2072.
(7) Drzaic, P. S. Recent Progress in Dichroic Polymer-Dispersed Liquid Crystal Materials. *Pure Appl. Chem.* **1996**, *68*, 1435−1440.
(8) Drzaic, P. S. Reorientation Dynamics of Polymer Dispersed Nematic Liquid Crystal Films. *Liq. Cryst.* **1988**, *3*, 1543−1558.
(9) Erdmann, J.; Doane, J. W.; Zumer, S.; Chidichimo, G. Electrooptic Response of PDLC Light Shutters. *Proc. SPIE* **1989**, *1080*, 32−40.
(10) Wu, B.-G.; Erdmann, J. H.; Doane, J. W. Response Times and Voltages for PDLC Light Shutters. *Liq. Cryst.* **1989**, *5*, 1453−1465.
(11) Chiccoli, C.; Pasini, P.; Skacej, G.; Zannoni, C.; Zumer, S. Dynamical and Field Effects in Polymer-Dispersed Liquid Crystals: Monte Carlo Simulations of NMR Spectra. *Phys. Rev. E* **2000**, *62*, 3766−3774.
(12) Golemme, A.; Zumer, S.; Doane, J. W.; Neubert, M. E. Deuterium NMR of Polymer Dispersed Liquid Crystals. *Phys. Rev. A* **1988**, *37*, 559−569.

(13) Buchert, K. L.; Koenig, J. L.; Wang, S. Q.; West, J. L. Molecular Motion Analysis of E7 in PDLCs as a Function of Droplet Size Using Solid-State ^{13}C NMR Relaxation Spectroscopy. *Appl. Spectrosc.* **1993**, *47*, 942−951.

(14) Ambrozic, M.; Formoso, P.; Golemme, A.; Zumer, S. Anchoring and Droplet Deformation in Polymer Dispersed Liquid Crystals: NMR Study in an Electric Field. *Phys. Rev. E* **1997**, *56*, 1825−1832.

(15) Kohri, S.; Kobayashi, J.; Tahata, S.; Kita, S.; Karino, I.; Yokoyama, T. Molecular Orientation in Polymer-Dispersed Liquid Crystals Using Time-Resolved FT-IR. *Appl. Spectrosc.* **1993**, *47*, 1367−1369.

(16) Hasegawa, R.; Sakamoto, M.; Sasaki, H. Dynamic Analysis of Polymer-Dispersed Liquid Crystal by Infrared Spectroscopy. *Appl. Spectrosc.* **1993**, *47*, 1386−1389.

(17) Jain, S. C.; Rout, D. K. Electrooptic Response of Polymer Dispersed Liquid-Crystal Films. *J. Appl. Phys.* **1991**, *70*, 6988−6992.

(18) Jain, S. C.; Thakur, R. S.; Lakshmikumar, S. T. Switching Response of a Polymer Dispersed Liquid-Crystal Composite. *J. Appl. Phys.* **1993**, *73*, 3744−3748.

(19) Amundson, K. Electrooptic Properties of a Polymer-Dispersed Liquid-Crystal Film: Temperature Dependence and Phase Behavior. *Phys. Rev. E* **1996**, *53*, 2412−2422.

(20) Amundson, K.; van Blaaderen, A.; Wiltzius, P. Morphology and Electro-Optic Properties of Polymer-Dispersed Liquid Crystal Films. *Phys. Rev. E* **1997**, *55*, 1646−1654.

(21) Mei, E.; Higgins, D. A. Local Dynamics in Polymer-Dispersed Liquid Crystals Studied by Near-Field Scanning Optical Microscopy. *Appl. Phys. Lett.* **1998**, *73*, 3515−3517.

(22) Mei, E.; Higgins, D. A. Near-Field Scanning Optical Microscopy Studies of Electric-Field-Induced Molecular Reorientation Dynamics. *J. Phys. Chem. A* **1998**, *102*, 7558−7563.

(23) Mei, E.; Higgins, D. A. Polymer-Dispersed Liquid Crystal Films Studied by Near-Field Scanning Optical Microscopy. *Langmuir* **1998**, *14*, 1945−1950.

(24) Mei, E.; Higgins, D. A. Electric-Field-Induced Ion Migration in Polymer-Dispersed Liquid-Crystal Films Observed by Near-Field Scanning Optical Microscopy. *Appl. Phys. Lett.* **1999**, *75*, 430−432.

(25) Mei, E.; Higgins, D. A. Nanometer-Scale Resolution and Depth Discrimination in Near-Field Optical Microscopy Studies of Electric-Field-Induced Molecular Reorientation Dynamics. *J. Chem. Phys.* **2000**, *112*, 7839−7847.

(26) Higgins, D. A.; Liao, X.; Hall, J. E.; Mei, E. Simultaneous Near-Field Optical Birefringence and Fluorescence Contrast Applied to the Study of Dye-Doped Polymer-Dispersed Liquid Crystals. *J. Phys. Chem. B* **2001**, *105*, 5874−5882.

(27) Hall, J. E.; Higgins, D. A. Exploring the Photorefractive Effect in Polymer-Dispersed Liquid Crystals Using Near-Field Scanning Optical Microscopy. *J. Phys. Chem. B* **2003**, *107*, 14211−14218.

(28) Hall, J. E.; Higgins, D. A. Photorefractive Polymer-Dispersed Liquid Crystals Studied by Near-Field Scanning Optical Microscopy. *Polym. Mater. Sci. Eng.* **2003**, *88*, 186−187.

(29) Hall, J. E.; Higgins, D. A. Exploring Dynamics in Photorefractive Polymer-Dispersed Liquid Crystals Using Near-Field Scanning Optical Microscopy. *ACS Symposium Series*, in press.

(30) Hall, J. E.; Higgins, D. A. Enhanced Photorefractivity from Ion-Doped Polymer-Dispersed Liquid Crystals. *J. Phys. Chem. B* **2004**, *108*, 16050−16055.

(31) Springer, G. H.; Higgins, D. A. Toroidal Droplet Formation in Polymer-Dispersed Liquid Crystal Films. *J. Am. Chem. Soc.* **2000**, *122*, 6801−6802.

(32) Luther, B. J.; Springer, G. H.; Higgins, D. A. Templated Droplets and Ordered Arrays in Polymer-Dispersed Liquid-Crystal Films. *Chem. Mater.* **2001**, *13*, 2281−2287.

(33) Higgins, D. A.; Luther, B. J. Watching Molecules Reorient in Liquid Crystal Droplets with Multiphoton-Excited Fluorescence Microscopy. *J. Chem. Phys.* **2003**, *119*, 3935−3942.

(34) Xie, A.; Higgins, D. A. Electric-Field-Induced Dynamics in Radial Liquid Crystal Droplets Studied by Multiphoton-Excited Fluorescence Microscopy. *Appl. Phys. Lett.* **2004**, *84*, 4014−4016.

(35) Dunn, R. C. Near-Field Scanning Optical Microscopy. *Chem. Rev.* **1999**, *99*, 2891−2927.

(36) Denk, W.; Strickler, J. H.; Webb, W. W. Two-Photon Laser Scanning Fluorescence Microscopy. *Science* **1990**, *248*, 73−76.

(37) Gratton, E.; Barry, N. P.; Beretta, S.; Celli, A. Multiphoton Fluorescence Microscopy. *Methods* **2001**, *00*, 103−110.

(38) Van de Hulst, H. C. *Light Scattering by Small Particles*; John Wiley and Sons: New York, 1957.

(39) Montgomery, G. P.; West, J. L.; Tamura-Lis, W. Light Scattering from Polymer-Dispersed Liquid Crystal Films: Droplet Size Effects. *J. Appl. Phys.* **1991**, *69*, 1605−1612.

(40) Drzaic, P. S. Droplet Density, Droplet Size, and Wavelength Effects in PDLC Light Scattering. *Mol. Cryst. Liq. Cryst. Sci. Technol., Sect. A* **1995**, *261*, 383−392.

(41) Gates, B.; Yin, Y.; Xia, Y. Fabrication and Characterization of Porous Membranes with Highly Ordered Three-Dimensional Periodic Structures. *Chem. Mater.* **1999**, *11*, 2827−2836.

(42) Yoshino, K.; Shimoda, Y.; Kawagishi, Y.; Nakayama, K.; Ozaki, M. Temperature Tuning on the Stop Band in Transmission Spectra of Liquid-Crystal Infiltrated Synthetic Opal as a Tunable Photonic Crystal. *Appl. Phys. Lett.* **1999**, *75*, 932−934.

(43) Mach, P.; Wiltzius, P.; Megens, M.; Weitz, D. A.; Lin, K.; Lubensky, T. C.; Yodh, A. G. Electrooptic Response and Switchable Bragg Diffraction for Liquid Crystals in Colloid-Templated Materials. *Phys. Rev. E* **2002**, *65*, No. 31720.

(44) Wiederrecht, G. In *Molecular and Supramolecular Photochemistry*; Schanze, K., Ramamurthy, V., Eds.; Marcel Dekker: New York, 2001; pp 319−362.

(45) Wiederrecht, G.; Yoon, B.; Wasielewski, M. High Photorefractive Gain in Nematic Liquid Crystals Doped with Electron Donor and Acceptor Molecules. *Science* **1995**, *270*, 1794−1797.

(46) Ostroverkhova, O.; Moerner, W. E. Organic Photorefractives: Mechanisms, Materials, and Applications. *Chem. Rev.* **2004**, *104*, 3267−3314.

(47) Santamaria, J. Solvent and Salt Effects. In *Photoinduced Electron Transfer. Part B. Experimental Techniques and Medium Effects*; Fox, M. A., Chanon, M., Eds.; Elsevier: Amsterdam, 1988; pp 483−540.

(48) Kawanishi, Y.; Kitamura, N.; Tazuke, S. Unexpected Salt Effects on Charge Separation Fields in Phenothiazine Derivatives-Methyl viologen Systems. *J. Phys. Chem.* **1986**, *90*, 6034−6037.